

*Full Length Research Paper*

# Investigation of structural properties of layered III-nitride semiconductor materials by high resolution X-rays diffraction

S. Ndiaye<sup>1\*</sup>, A. Dioum<sup>1</sup>, P. D. Tall<sup>1</sup>, K. Bejtka<sup>2</sup>, M. Laugt<sup>3</sup>, H. P. D. Schenk<sup>3,4</sup> and A. C. Beye<sup>1</sup>

<sup>1</sup>Groupe de Laboratoires de Physique des Solides et Sciences des Matériaux, Département de Physique, Faculté des Sciences et Techniques Université Cheikh Anta Diop, Dakar, Sénégal.

<sup>2</sup>Center for Space and Human Robotics, Italian Institute of Technology (IIT@PoliTO), Corso Trento 21, 10129 Torino, Italy.

<sup>3</sup>CRHEA-CNRS, Rue Bernard Gregory, Sophia-Antipolis, 06560 Valbonne, France.

<sup>4</sup>PICOGIGA International, Place Marcel Rebuffat, Parc de Villejust, 91971 Courtaboeuf, France.

Accepted 6 January, 2012

**High resolution X-ray diffraction (HRXRD) was used to investigate the structural properties of group III-nitride semiconductors, and was shown to give separable information on crystalline quality as well as on chemical composition, residual stresses, etc. Contributions from the various structural parameters to the HRXRD diagram profile, although mixed to each other, have been sorted out. Through the examples of GaN/In<sub>x</sub>Al<sub>1-x</sub>N/GaN heterostructures and Al<sub>x</sub>Ga<sub>1-x</sub>N/GaN superlattices (SLs), grown by metal-organic chemical vapour deposition, it has been shown that all the structural parameters of III-nitrides are deducible from HRXRD combined with simulation methods.**

**Key words:** X-ray diffraction, heterostructure, superlattice, III-nitride, lattice parameter, relaxation state.

## INTRODUCTION

Group III-nitride (III-N) hexagonal semiconductors have band gaps spanning the entire visible and near ultraviolet (UV) ranges (from 0.7 eV for InN to 6.3 eV for AlN) (Hangleiter et al., 1999; Novikov et al., 2011). III-N materials (GaN, InN, AlN and their related alloys) are also known for their high thermal stability (Ambacher et al., 1996; Levander et al., 2011). Thanks to such properties, those semiconductors are suitable for solid state lightning (blue-green light-emitting diodes and laser diodes), high electron mobility transistors and other optoelectronic applications, where silicon technology fails (Nakamura et al., 1994; Ohta et al., 2007). However, the lack of native substrate is a crucial problem for the growth of III-N films. Indeed, usual substrates (silicon or sapphire) have lateral

lattice parameters and thermal expansion coefficients differing from those of III-N materials, therefore inducing strain and other defects. The analysis of such defects is a challenge if one aims to optimize the growth conditions for good quality materials. X-ray diffraction is a well-established non-destructive technique for defects monitoring in thin films and multilayers. Furthermore, X-ray diffraction can provide information on lattice parameters, thickness, composition, etc. However, all of these contributions to the X-ray diffraction line profiles are often mixed in a somehow complex way. Therefore, simulation methods are essential in any profile analysis. Despite of numerous publications on the topic (Moram and Vickers, 2009; Wilson, 2006; Herres et al., 2002), the X-ray diffraction profile analysis needs additional investigation.

This paper presents a study of the structural properties of III-N thin films and superlattices (SLs) by high resolution X-ray diffraction (HRXRD). Structures under

\*Corresponding author. E-mail: [sossendiaye@yahoo.fr](mailto:sossendiaye@yahoo.fr). Tel: +221 650 32 52. Fax: +221 33 824 63 18.

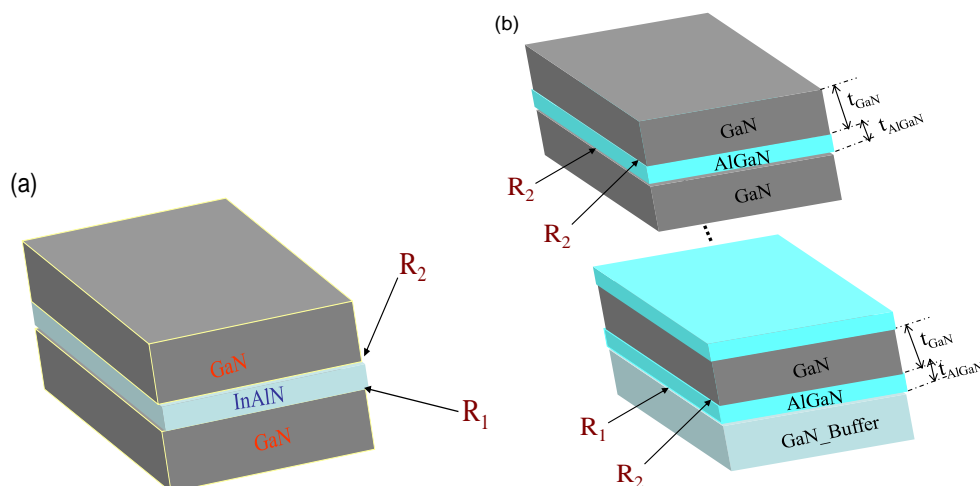


**Figure 1.** Schematics of (a) homoepitaxial GaN with AlInN insertion layer and (b) superlattice AlGaIn/GaN on GaN bulk or buffer. R1 and R2 stand for the strain states corresponding to indicated interfaces.

investigation are  $\text{Al}_x\text{Ga}_{1-x}\text{N}/\text{GaN}$  (AlGaIn) superlattices (SLs) and homoepitaxial GaN with inserted  $\text{In}_x\text{Al}_{1-x}\text{N}$  (InAlN) ultra thin buffer layer. III-N alloys are commonly used: (1) to enhance the confinement-based electron-mobility in field effect transistor, (2) to provide a contrast of optical refractive index for distributed Bragg reflectors and (3) for cladding layers in GaN-based laser structures. However, alloys grown on GaN are under biaxial strain and tend, in thick layers, to release the strain energy throughout formation of cracks (dislocations) (Pereira et al., 2002). AlGaIn/GaN SLs with short period are suitable instead of bulk AlGaIn layers. In such structures, GaN wells and AlGaIn barriers thicknesses remain below their critical values, where relaxation occurs.

The chemical composition, thickness and strain state of targeted materials were derived, from experimental HRXRD profiles by iterative simulations.

## EXPERIMENTAL PROCEDURE

### Samples preparation

$\text{GaN}/\text{In}_x\text{Al}_{1-x}\text{N}/\text{GaN}$  (Figure 1a) were grown by metal-organic vapour phase epitaxy in an Aixtron 200-series reactor, using trimethylgallium (TMGa), trimethylaluminium (TMAI), trimethylindium (TMIn) and ammonia as respective precursors for gallium, aluminium, indium and nitrogen sources. The growth sequence starts with a 500 nm GaN buffer layer, followed by a 70 nm nominal  $\text{In}_{0.17}\text{Al}_{0.83}\text{N}$ , and finally 500 nm more of GaN. The InAlN was grown at a set-point temperature of 840°C and 75 mbar pressure in a nitrogen ambient, whereas both GaN layers were grown at 1140°C and 200 mbar pressure in a hydrogen ambient (Bejtka et al., 2006). The  $\text{GaN}/\text{In}_x\text{Al}_{1-x}\text{N}/\text{GaN}$  structures referred to as sample A and sample B were grown during the same growth run. Sample A was grown on a double polished free standing

(FS)-GaN substrate from Lumilog-France (Vallauris France). The starting substrate for sample B consists of a 4  $\mu\text{m}$  thick GaN, previously grown on c-plane sapphire in our Aixtron reactor. In this study, the quality of the top GaN layer in samples A and B have been compared to that of our home made GaN-on-sapphire (sample C), and reference FS-GaN from Lumilog (sample D).

AlGaIn/GaN SLs (Figure 1b) were grown by metal-organic chemical vapour deposition method, in a 4 × 2" Thomas Swan reactor using TMGa, TMAI and ammonia as gas precursors. Several structures have been deposited on bulk GaN and sapphire substrates prior to the AlGaIn/GaN SLs deposition. More details on the initial stages of growth are reported in Schenk et al. (2002, 2005). The growth of the SLs consisted in deposition of alternative AlGaIn and GaN layers. Sample (S1) consists nominally of 70 asymmetric periods of GaN well (~30Å) and AlGaIn barrier (~70Å) with a nominal aluminium content of 10%. Then in S1, the predicted average value for aluminium content is ~7% and the structure is summarized as follow:  $[\text{30}\text{\AA}.\text{GaN}/\text{70}\text{\AA}.\text{Al}_{0.10}\text{Ga}_{0.90}\text{N}]^{70}$ . Three other samples were grown, which consisted of 70 periods of GaN well (25Å) and AlGaIn barrier (60Å) with nominal aluminium average composition of 7% for S2  $[\text{25}\text{\AA}.\text{GaN}/\text{60}\text{\AA}.\text{Al}_{0.10}\text{Ga}_{0.90}\text{N}]^{70}$  and 10% for S3 and S4:  $[\text{25}\text{\AA}.\text{GaN}/\text{60}\text{\AA}.\text{Al}_{0.14}\text{Ga}_{0.86}\text{N}]^{70}$ . Substrates [(0001) oriented] used for SLs growth were either bulk (ultra low defects density) GaN (for S1 and S3) or 11  $\mu\text{m}$  thick GaN buffer deposited on sapphire (for S2 and S4).

### Techniques of analysis and simulation methods

HRXRD measurements were carried out using a *Bede D<sup>3</sup> System* equipped with a compact two-crystal Silicon (220) monochromator which produces a well collimated and parallel monochromatic  $\text{CuK}\alpha_1$  X-ray beam. The resolution is ~12 arcsec in  $\theta$  angle. Measurements on sample S3 were done with a Seifert PTS3003, equipped with a 2 bounces Germanium (220) analyser. Bragg angles from the Seifert equipment were used as a reference in order to subtract the instrumental contribution from the HRXRD profiles. For all measurements, room temperature was set at the constant value of 21°C.

Indications on the composition and crystalline quality of samples were deduced from rocking curves. Experimental in-plane ( $a_{\text{measured}}$ ) and vertical ( $c_{\text{measured}}$ ) lattice parameters for both GaN and alloy layers are derived from a set of symmetric and asymmetric rocking curves (Bond, 1960; Fewster and Andrew, 1995). The indium (or aluminium) concentration ( $x_{\text{measured}}$ ) is deduced from the intersect of the theoretical plots of  $\frac{c_{\text{measured}}}{c_0(x)} - 1 = f(x)$  and

$$\frac{C_{13}}{C_{33}} \left[ 1 - \frac{a_{\text{measured}}}{a_0(x)} \right] = g(x)$$

Where  $a_0(x)$  and  $c_0(x)$  stand for the strain-free lattice parameters of the alloy calculated assuming the linear Vegard's law;  $C_{ij}$  are the elastic constants of material under consideration (Polian et al., 1996). The experimental strain-free lattice parameters ( $a_{0\text{measured}}$ ,  $c_{0\text{measured}}$ ) are then derived and the real state of strain ( $R = \frac{a_{\text{measured}} - a_{\text{strained}}}{a_{0\text{measured}} - a_{\text{strained}}}$ ) deduced (Kisielewski et al., 1996). Basically, for mismatched alloys grown on GaN films, the fully strained in-plane lattice parameter ( $a_{\text{strained}}$ ) is supposed to

equate the lateral lattice parameter of GaN. Furthermore, comparison between measured and calculated values of symmetric Bragg peak separations leads to an accurate estimate of the strain state. Indeed, usual behaviour for mismatched epilayers is, for thin layers, to be fully strained (and pseudomorphic) to the supporting material up to a critical thickness (Einfeldt et al., 2001; Pereira et al., 2002). Beyond this threshold of thickness, relaxation starts in the layer and the peak separation decreases or increases, depending on the nature of both the layer and substrate. In AlGaIn/GaN structures, the lateral lattice parameter of the alloy ( $a_{\text{AlGaIn}}$ ) is smaller than the corresponding one in the substrate (GaN). If the alloy is fully strained, the two in-plane lattice parameters equate to each other. The so-generated lateral strain induces a contraction of the vertical lattice parameter ( $c_{\text{AlGaIn}}$ ) of the alloy, which results in increasing the Bragg angle ( $\theta$ ) of the alloy. Thus, the peak separation is larger in fully-strained alloy than in partially-strained or unstrained ones.

On a HRXRD ( $2\theta-\omega$ ) diagram, the superlattice effect appears as additional peaks or satellites, dealing with the existence of a super period (Khapachev, 1983). In this study, the method used for SLs characterization is described as follows, and consists mainly in four steps in which the spacing period (T), the strain state (R), the chemical composition (x) and the sub layers characteristics parameters are successively determined.

**First step: Determination of the space period (T) of a superlattice**

The spacing or period (T) of a superlattice is the thickness of its constitutive unit: e.g.  $T = t_{\text{AlGaIn}} + t_{\text{GaN}}$  as shown in

Figure 1b. Starting with Bragg's law, one can express the period as a function of the angular positions of satellite peaks in a ( $2\theta-\omega$ ) diagram (Figure 3). T is related to the reflexion order (n) of a satellite by:

$$T = \frac{n\lambda}{2\sin\theta_n}$$

where  $\theta_n$  and  $\lambda=1.54056\text{\AA}$  are the satellite peak position (Bragg angle) and X-ray radiation wavelength, respectively. For SLs grown along the c-direction, the symmetric inter-planar distance  $d_{00\ell}$  is

given by:  $c = \ell d_{00\ell}$ ; where  $\ell \equiv n$ . The average out-of-plane lattice parameter  $\langle c \rangle$  of a superlattice equals its spacing period T. The reflexion order n is deduced to be:

$$n = \frac{d_{n+j}}{d_{n-i} - d_{n+j}}(i+j) + i = \frac{\frac{T}{n+j}}{\frac{T}{n-i} - \frac{T}{n+j}}(i+j) + i$$

where i and j stand for the satellites orders. For  $i=-1$  and  $j=+1$ , T is calculated as follows:

$$T_{\text{measured}} = \lambda \frac{\sin\theta_{+1} + \sin\theta_{-1}}{2\sin\theta_0(\sin\theta_{+1} - \sin\theta_{-1})}$$

**Second step: Relaxation state  $R_1(\text{AlGaIn}/\text{GaN}_{\text{Buffer}})$  and  $R_2(\text{GaN}_{\text{Sublayer}}/\text{AlGaIn})$**

When a superlattice with pseudomorphic sub-layers is free of stress from its supporting substrate ( $R_1 = 100\%$ ), the satellites of same order (+n) and (-n) are symmetrical around the main peak SR0 and have equal intensities. If a tensile strain ( $\epsilon_a > 0$ ) is applied, the satellite (-n) is higher in intensity than the (+n) one; reversely, for negative (compressive) strain, the satellite (-n) has lower intensity than (+n). The relaxation state is deduced from HRXRD measurements by the following procedure:

First, the average lattice parameters  $\langle c \rangle$  and  $\langle a \rangle$  are theoretically expressed as a function of the average aluminium concentration  $\langle x \rangle$ .

Instead of the absolute lattice parameters, the ratio  $\langle c \rangle / \langle a \rangle$  is used in a modified Vegard's rule in order to take into account the full effect of the strain on the structure. One shall consider a given couple ( $t_{\text{AlGaIn}}$ ;  $t_{\text{GaN}}$ ) of AlGaIn and GaN sub-layers thicknesses, and some arbitrary values for  $\langle x \rangle$  to generate the theoretical graph of  $\langle c \rangle / \langle a \rangle = Q(\langle x \rangle)$ . This graph (a straight line) can be shifted when tuning  $R_1$  and  $R_2$ . Second, the experimental point ( $\langle c_{\text{measured}} \rangle / \langle a_{\text{measured}} \rangle$ ;  $x_{\text{nominal}}$ ) is plotted on the same graph;  $x_{\text{nominal}}$  is the average value of Al concentration estimated from the growth rate. Third, taking into account the satellite peak shapes and positions, adjust  $R_1$  and  $R_2$  to fit the experimental point with the theoretical curve. A first evaluation of  $R_1$  and  $R_2$  is done at this point. Iterative refinement of these values will be performed later.

**Third step: Determination of the experimental average Al concentration  $\langle x_{\text{measured}} \rangle$**

A graphical method similar to the one described earlier for the strain is used to deduce the average aluminium concentration: First, for a given value of  $\langle x \rangle$ , one considers some arbitrary values of the spacing  $T = t_{\text{AlGaIn}} + t_{\text{GaN}}$  in order to generate and plot the graph  $\langle c \rangle / \langle a \rangle = P(T)$ . Second, put the experimental point ( $\langle c_{\text{measured}} \rangle / \langle a_{\text{measured}} \rangle$ ;  $T_{\text{measured}}$ ) onto the obtained theoretical graph;  $T_{\text{measured}}$  is the above determined period of the superlattice. Third, tune the value of  $\langle x \rangle$  to match the experimental point with the theoretical graph. The average Al concentration  $\langle x_{\text{measured}} \rangle$  is deduced and will be refined.

**Fourth step: Thicknesses ( $t_{\text{AlGaIn}}$  and  $t_{\text{GaN}}$ ) and Al concentration in AlGaIn monolayers**

The experimental concentration of aluminium in individual AlGaIn

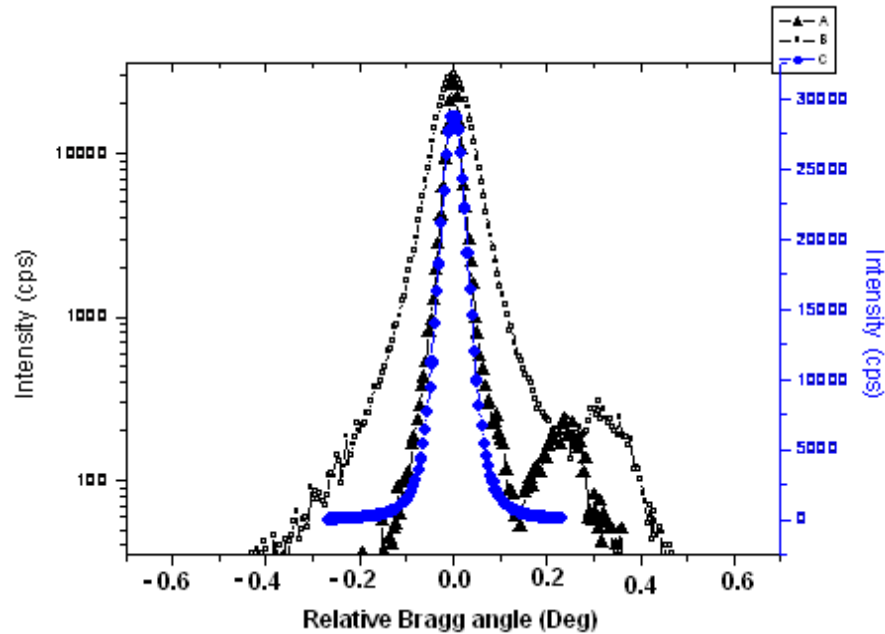


**Figure 2.** Rocking curves of samples A, B and template GaN/Sapphire (C), with (0002) GaN peak as reference position for relative Bragg angles ( $\Delta\omega$ ).

sub-layer is given by:  $x_{measured} = \frac{\langle x_{measured} \rangle T_{measured}}{t_{AlGaN}}$ . From the estimated values of  $t_{AlGaN}$  and  $t_{GaN}$ , the lattice parameters  $a(AlGaN)$ ,  $a(GaN)$ ,  $c(AlGaN)$  and  $c(GaN)$  for individual sub-layers of AlGaN and GaN can be calculated and the corresponding thicknesses deduced by the following relations:

$$\begin{cases} t_{AlGaN} = T_{measured} \frac{\langle a_{measured} \rangle c_{(GaN)} - \langle c_{measured} \rangle a_{(GaN)}}{a_{(AlGaN)} \cdot c_{(GaN)} - a_{(GaN)} \cdot c_{(AlGaN)}} \\ t_{GaN} = T_{measured} - t_{AlGaN} \end{cases}$$

Screw dislocation densities are calculated using the slope ( $\alpha_\omega$ ) of  $\beta\omega \frac{\sin\theta}{\lambda}$  plotted as a function of  $\frac{\sin\theta}{\lambda}$ ; where  $\beta_\omega$ ,  $\theta$  and  $\lambda$  stand, respectively for the FWHM (Pearson VII fit model), the Bragg angle and the exciting wave length (Booker et al., 2010; Chierchia et al., 2003). Dislocation densities have also been estimated by imaging and counting the emerging pits at the surface of the samples. Counts were done on sampled squares ( $4 \times 4 \mu m^2$ ) within an overall area of  $\sim 100 \mu m^2$ .

**RESULTS AND DISCUSSION**

**Epitaxial GaN with InAlN insertion layer**

Figure 2 displays the (0002) peaks of HRXRD rocking curves, measured for samples A, B and D. Each of A and B exhibit a single characteristic peak for GaN (0002) reflection. Since X-ray penetration depth is larger than the top GaN and underlying InAlN overall thickness, the

strain state is assumed to be identical for both buffer and cap GaN layers:  $R1 = R2$ .

Table 1 lists the peak separations of rocking curves for samples A and B. The corresponding theoretical values for fully relaxed and almost fully-strained materials are also given for comparison. Measured peak separations for A ( $\sim 890$  arcsec) is fairly similar to that of fully relaxed alloys. For B, the peak separation ( $\sim 1170$  arcsec) intermediates those of fully-relaxed and totally-strained alloys, although closer to the latter. Qualitative conclusion that can be deduced from these results is that the alloy and GaN layers are strain-free in sample A ( $R1 \approx 100\%$ ) and partially strained in B.

According to linear Vegard's rule and from intersects of  $f(x)$  and  $g(x)$ , respective values of indium concentration ( $x_{measured}$ ) of  $\sim 17$  and  $\sim 16.5\%$  for A and B are obtained. These values are closed to those predicted for InAlN pseudomorphic to GaN. The strain-free lattice parameters ( $a_{0measured}$ ,  $c_{0measured}$ ) are then calculated. Furthermore, experimental lattice parameters of the alloy ( $a = 3.1896\text{\AA}$ ,  $c = 5.1142\text{\AA}$  for A and  $a = 3.1842\text{\AA}$ ,  $c = 5.0956\text{\AA}$  for B) are obtained from a set of symmetric and asymmetric rocking curves (Bond, 1960; Fewster and Andrew, 1995). The strained state is then deduced to be  $R1 = 30\%$  for sample B.

The aforementioned results are corroborated by the full widths at half maximum (FWHMs) of GaN (0002) rocking curves. Single peaks with line width of  $\sim 100$  arcsec (sample A) and  $260$  arcsec (B) are obtained. These values are compared to those of respective

**Table 1.** Measured values of separation (in arcsec) between GaN and  $\text{In}_x\text{Al}_{1-x}\text{N}$  (0002) Bragg peaks, for samples.

Sample	Strain-free (Lattice matched)	“Fully” strained (R = 5%)	This study
A	895	950	890
B	1050	1200	1170

A [GaN(500 nm)/ $\text{In}_x\text{Al}_{1-x}\text{N}$ (70 nm)/GaN(500 nm)/FS-GaN] and B: [GaN(500 nm)/ $\text{In}_x\text{Al}_{1-x}\text{N}$ (70 nm)/GaN(500 nm)/GaN(4  $\mu\text{m}$ )/Sapphire]. Theoretical values for totally relaxed and fully strained materials are added for comparison.

**Table 2.** Values of the full widths at half maximum (FWHM) for GaN (0002) Bragg peak in the cases of samples.

Sample	Rocking curves (0002) FWHM (arcsec)
A	104
B	260
C	250
D	110

A [GaN(500 nm)/ $\text{In}_x\text{Al}_{1-x}\text{N}$ (70 nm)/GaN(500nm)/FS-GaN]; B: [GaN(500 nm)/ $\text{In}_x\text{Al}_{1-x}\text{N}$ (70 nm)/GaN(500nm)/GaN(4 $\mu\text{m}$ )/Sapphire]; and C [GaN(4 $\mu\text{m}$ )/Sapphire]; D [FS-GaN].

corresponding structures, D (110 arcsec) and C (250 arcsec), without InAlN inserted layer (Table 2). HRXRD line widths confirmed that the InAlN inserted layer does not alter the structural quality of cap GaN. Indeed, structural quality of GaN in samples A and B is comparable, respectively to FS-GaN and buffer GaN grown on sapphire (C) which is known to be traditionally under biaxial compression. No additional strain has been generated by the insertion of the alloy. Top and buffer GaN in sample A are strain-free as expected for GaN pseudomorphically stacked on InAlN.

The results finally indicate that the inserted InAlN is lattice-matched to GaN, and does not induce additional defects or internal strain. The method gave accurate values for the chemical composition and strain of the structures.

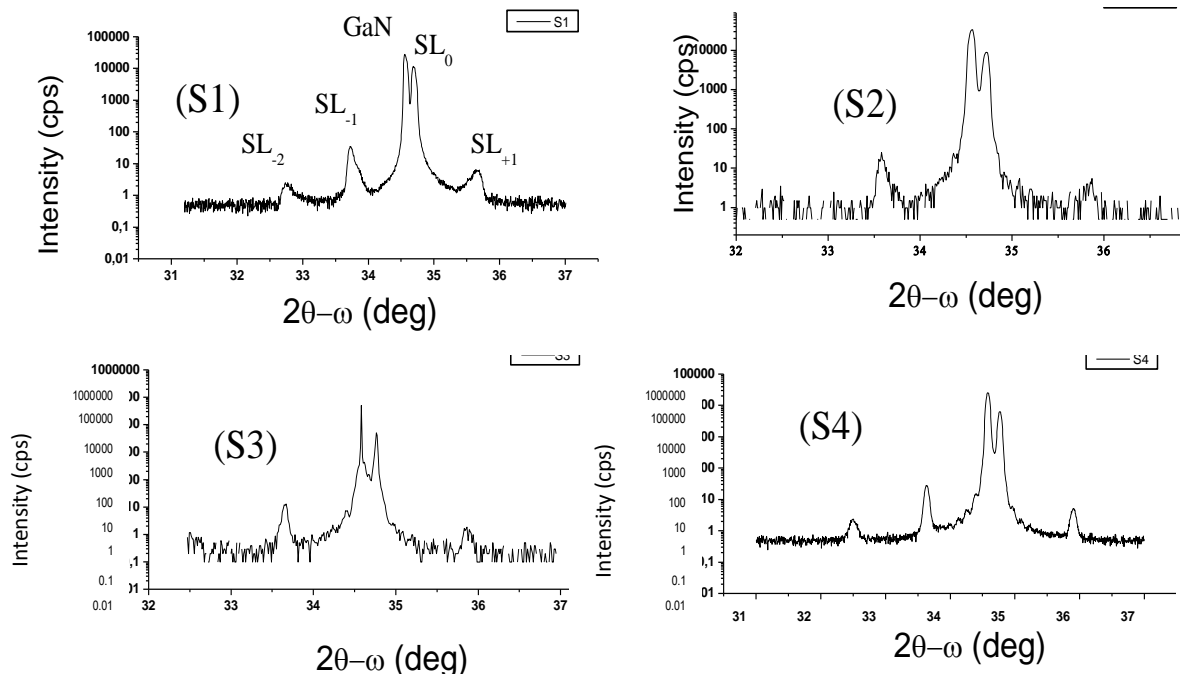
### AlGaIn/GaN super lattices (SLs)

Figure 3 displays a  $(2\theta-\omega)$  HRXRD diagram of our four SLs. It consists of the GaN (0002) Bragg peak from the substrate, surrounded by the main (SL0) and satellite peaks (SL1, SL-1...) from the superlattice. The presence of the first and second order reflections, in addition to the zero order one, is an indication of good crystalline quality of the structures. For all samples, the intensity of the left-side first order satellite peak (SL<sub>-1</sub>) is larger than that of the right-side one (SL<sub>+1</sub>), meaning that AlGaIn/GaN SLs are under tensile stress onto the GaN buffer. The narrow

line widths (~120 arcsec) of the SLs central peaks (SL0) suggest that the interfaces are very sharp. Experimental values of the SLs periods, sub-layer thicknesses and Al compositions deviate from predictions (Table 3). In the same trend, the first order satellites (SL<sub>-1</sub> and SL<sub>+1</sub>) are broader than the zero order (SL0) peak, which indicates that the spacing and/or the Al concentration fluctuate throughout the structures. Furthermore, the second order satellites (if observable like in S1 and S4) were twice broader than the first order satellites. We then considered that variation of the spacing periods throughout the structures is dominant in our SLs as compared to the gradients of Al composition.

Table 3 summarizes the measured and calculated values of the characteristic parameters of samples S1-4. Simulated X-ray diffraction curves from these values are consistent with experimental ones. An example is as shown in Figure 4, which sketches the measured and simulated  $(2\theta-\omega)$  curves for sample S1.

Compared to the dislocation density in the virgin substrate ( $\sim 10^8 \text{ cm}^{-2}$ ), a slight reduction have been observed in AlGaIn/GaN SLs grown on buffer GaN/sapphire, whatever the aluminium content (namely, 7% for S2 or 10% for S4). The measured dislocation density remained in the order of several  $10^7 \text{ cm}^{-2}$ . S2 and S4 have similar dislocation densities despite the highest Al concentration in S4. Such behaviour is tentatively related to the fact that an increase of the Al concentration in AlGaIn barriers lowers the critical layer thickness for strain relaxation. Thus, a strain release might have



**Figure 3**

**Figure 3.**  $(2\theta-\omega)$  HRXRD diagrams of AlGaIn/GaN SLs: (S1)  $[30\text{\AA}.GaN/70\text{\AA}.Al_{0.10}Ga_{0.90}N]^{70}$ , (S2)  $[25\text{\AA}.GaN/60\text{\AA}.Al_{0.10}Ga_{0.90}N]^{70}$ , (S3)  $[25\text{\AA}.GaN/60\text{\AA}.Al_{0.14}Ga_{0.86}N]^{70}$  and (S4)  $[25\text{\AA}.GaN/60\text{\AA}.Al_{0.14}Ga_{0.86}N]^{70}$ .

**Table 3.** Values of the FWHMs of SL main (0002) peak SL0, experimental average aluminum concentration  $\langle x \rangle$ , superlattices periods T, individual layers thicknesses ( $t_{AlGaIn}$  and  $t_{GaN}$ ) and screw dislocation densities (Ns) for samples S1 to 4.

	<b>S1</b>	<b>S2</b>	<b>S3</b>	<b>S4</b>
$\langle x \rangle$ (%)	7 <sup>(a)</sup> 7.1	7 <sup>(a)</sup> 8.6	10 <sup>(a)</sup> 9.8	10 <sup>(a)</sup> 10.2
Period T (Å)	100 <sup>(a)</sup> 103	85 <sup>(a)</sup> 81	85 <sup>(a)</sup> 84	85 <sup>(a)</sup> 82
$t_{AlGaIn}$ (Å)	70	56	59	57
$t_{GaN}$ (Å)	33	25	25	25
$n_{AlGaIn}$	14	11	12	11
$n_{GaN}$	6	5	5	5
FWHM for SL0 (arcsec)	122	124	110	119
Ns ( $10^7 \text{ cm}^{-2}$ )	3 <sup>(b)</sup> 5.88	9.7 <sup>(b)</sup> 8.46	6 <sup>(b)</sup> -	8.2 <sup>(b)</sup> 7.7

The subscript <sup>(a)</sup> stands for predicted values from growth conditions and <sup>(b)</sup> indicates dislocation densities deduced by AFM.  $n_{AlGaIn}$ ,  $n_{GaN}$  are respective numbers of AlGaIn and GaN monolayers in a period.

occurred via dislocations. We deduced that preservation of crystalline quality in S4 is related to the short spacing

period. The FWHMs of SL0 peak for our different samples followed the same trend, concerning the crystal

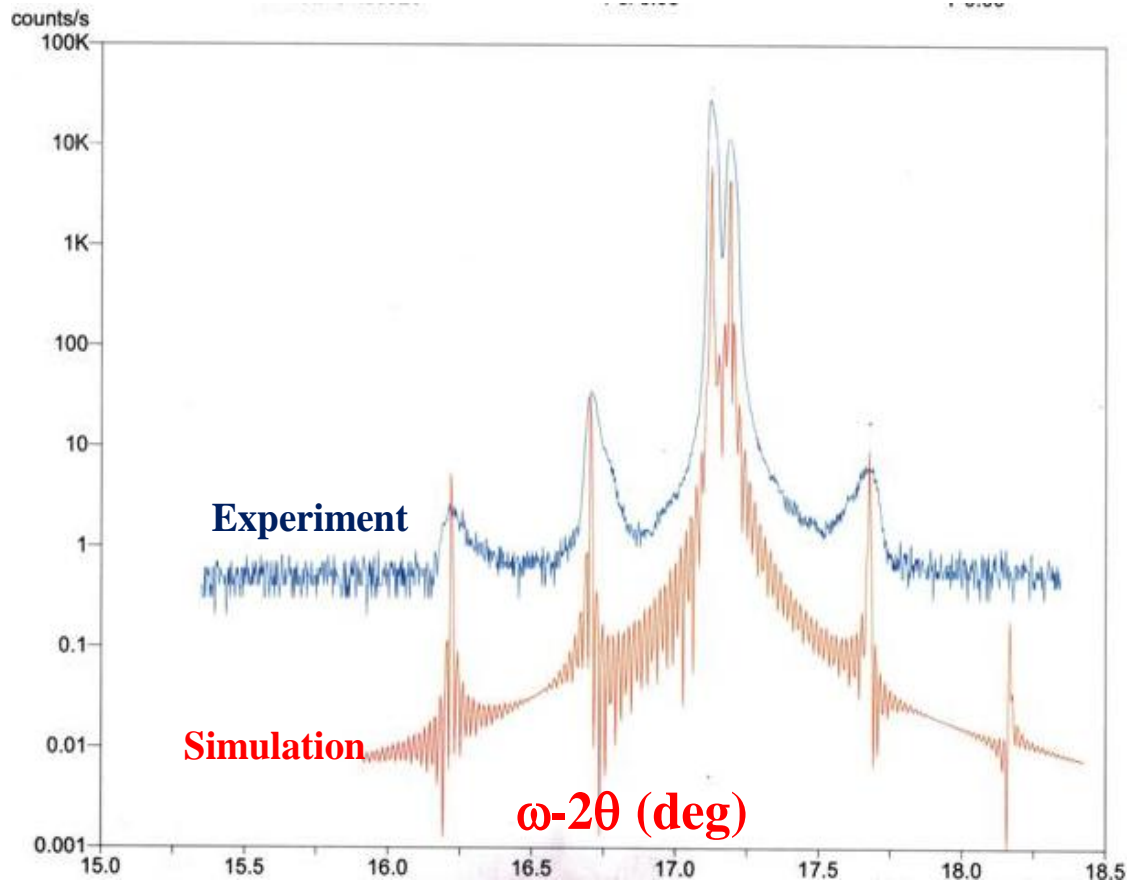


**Figure 4.** Comparison between experimental and simulated ( $2\theta$ - $\omega$ ) HRXRD diagrams for sample S1:  $[30\text{\AA}.GaN/70\text{\AA}.Al_{0.10}Ga_{0.90}N]^{70}$ .

packing. This result is consolidated by the observed relative quality degradation in S1, although grown on free-standing GaN, with the same nominal aluminium concentration as S2 (7%). Such degradation might probably originate from the large spacing period throughout the overall SL.

## Conclusion

HRXRD confirms that inserting  $In_xAl_{1-x}N$  ( $x \sim 16.5$  to  $17\%$ ) preserves the crystalline quality of overgrown GaN. Through the example of AlGaIn/GaN SLs, it is shown that almost all the structural parameters of SLs are deducible from HRXRD results, although their contributions on the peak profiles are mixed. Possible fluctuation in thickness and chemical composition are emphasized to be considered when analysing the diffraction line profile. HRXRD is shown to be an indicated technique for post growth control of the structure, composition and crystalline quality in (0001) oriented III-N heterostructures.

## REFERENCES

- Ambacher O, Brandt MS, Dimitrov R, Metzger T, Stutzmann M, Fischer RA, Miehr A, Bergmaier A, Dollinger G (1996). Thermal stability and desorption of Group III nitrides prepared by metal organic chemical vapor deposition. *J. Vac. Sci. Technol.*, B 14: 3532 - 3542.
- Bejtka K, Martin RW, Watson IM, Ndiaye S, Leroux M (2006). Growth and optical and structural characterization of GaN on free-standing GaN substrates with an (Al,In)N insertion layer. *Appl. Phys. Lett.*, 89: 191912.
- Bond WL (1960). Precise lattice constant determination. *Acta Crystallogr.*, 13: 814-818.
- Booker I, Rahimzadeh Khoshroo L, Weitok JF, Kaganer V, Mauder C, Behmenburg H, Gruis J, Heuken M, Kalisch H, Jansen RH (2010). Dislocation density assessment via X-ray GaN rocking curve scans. *Phys. Status Solidi (c)* 7(7-8): 1787-1789.
- Chierchia R, Bottcher T, Heinke H, Einfeldt S, Figger S, Hommel D (2003). Microstructure of heteroepitaxial GaN revealed by X-ray diffraction. *J. Appl. Phys.*, 93: 8918-8925.
- Einfeldt S, Heinke H, Kirchner V, Hommel D (2001). Strain relaxation in AlGaIn/GaN super lattices grown on GaN. *J. Appl. Phys.*, 89: 2160-2167.
- Fewster PF, Andrew NL (1995). Absolute lattice parameter measurement. *J. Appl. Cryst.* 28: 451-458.
- Hangleiter A, Duboz J-Y, Kishino K, Ponce FA (1999). In Proceedings of Symposium L on Nitrides and related wide band gap materials. European Material Research Society Symposia Proceedings, p. 423.
- Herres N, Kirste N, Obloh H, Köhler K, Wagner J, Koidl P (2002). X ray

- determination of the composition of partially strained group III nitride layers using extended bond method. *Mater. Sci. Eng.*, B91-92: 425-432.
- Khapachev YP (1983). Theory of dynamical X ray diffraction on a superlattice. *Phys. Status Solidi (b)*, 120: 155-163.
- Kisielewski C, Krüger J, Ruvimov S, Suski T, Ager JW, Jones E, Liliental-Weber Z, Rubin M, Weber ER, Bremser MD and Davis RF (1996). Strain related phenomena in GaN thin films. *Phys. Rev.*, B54: 17745-17753.
- Levander AX, Broesler R, Liliental-Weber Z, Novikov SV, Foxon CT, Dubon OD, Wu J, Walukiewicz W, Yu KM (2011). Thermal Stability of Amorphous GaN<sub>1-x</sub>As<sub>x</sub> Alloys. *Appl. Phys. Lett.*, 98: 161902-161902-3.
- Moram MA, Vickers ME (2009). X-ray diffraction on III-Nitrides. *Rep. Prog. Phys.*, 72: 036502 (40 pp).
- Nakamura S, Mukai T, Senoh M (1994). Candela-class high brightness InGaN/AlGaIn double-heterostructure blue-light-emitting diodes. *Appl. Phys. Lett.*, 64(13): 1687-1689.
- Novikov SV, Staddon CR, Foxon CT, Yu KM, Broesler R, Hawkrige M, Liliental-Weber Z, Denlinger J, Demchenko I, Luckert F, Edwards PR, Martin RW, Walukiewicz W (2011). Growth by Molecular Beam Epitaxy of amorphous and crystalline GaNAs alloys with band gaps from 3.4eV to 0.8eV for solar energy conversion devices. *J. Cryst. Growth*, 323: 60-63.
- Ohta M, Ohizumi Y, Hoshina Y, Tanaka T, Yabuki Y, Funato K, Tomiya S, Goto S, Ikeda M (2007). High-power pure blue laser diodes. *Phys. Status Solidi (a)* 204(6): 2068-2072.
- Pereira S, Correia MR, Pereira E, Trager-Cowan C, Sweeney S O'Donnell KP (2002). Structural and optical properties of InGaN/GaN layers close to the critical layer thickness. *Appl. Phys. Lett.*, 81: 1207-1209.
- Polian A, Grimsditch M, Grzegory I (1996). Elastic constants of gallium nitride. *J. Appl. Phys.*, 79: 3343-3344.
- Schenk HPD, Czernecki R, Krowicki K, Targowski G, Wisniewski P, Grzanka S, Krysko M, Tottereau O, Vennéguès P, Perlin P, Leszczynski M, Suski T (2005). Growth of GaN/Al<sub>x</sub>Ga<sub>1-x</sub>N-based Bragg reflectors on sapphire and bulk GaN substrates by metalorganic chemical vapor deposition: Towards group III-nitride microcavities. *Proc. 9th Ann. Nanophys. Nanoel. Symp.*, pp. 338-339.
- Schenk HPD, de Mierry P, Vennéguès P, Tottereau O, Laügt M, Vaillie M, Feltn E, Beaumont B, Gibart P, Fernández S, Calle F (2002). *In situ* growth monitoring of distributed GaN-AlGaIn Bragg reflectors by metalorganic vapor phase epitaxy. *Appl. Phys. Lett.*, 80: 174-176.
- Wilson AJC (2006). Determination of lattice parameters. *Int. Tables Crystallogr.*, Berlin-Springer, 28: 110.